Al-Doped ZnO Nanowires by Electrochemical Deposition for Selective VOC Nanosensor and Nanophotodetector

Thierry Pauporté,* Oleg Lupan,* Vasile Postica, Mathias Hoppe, Lee Chow, and Rainer Adelung

Nanomaterials for new nanosensor systems with selective detection of hazardous volatile organic compounds (VOCs) vapors are of great demand nowadays. In this paper, the use in nanosensors of electrochemically deposited (ECD) Al-doped ZnO (ZnO:Al) nanowires (NWs) is reported. The NWs are characterized by micro-Raman and optical measurements. Individual ZnO and ZnO:Al NWs are integrated into nanosensor devices for room temperature UV and gas sensing. It is shown that, compared to undoped ZnO NW with irreversible response, the doped ZnO:Al NWs have faster response ($\approx$5 s) and recovery ($\approx$55 s), as well as enhanced UV response ($\approx$4.8, about 2 times higher). The room temperature gas sensing investigations demonstrate that an individual ZnO:Al NW can detect volatile organic compounds (VOCs) vapors such as 2-propanol, n-butanol and ethanol at room temperature with a relatively fast response time of $\approx$10 s and a reversible signal (the recovery time being 30–40 s). This shows the possibility to use it with further development as indoor air quality monitor.

1. Introduction

Due to regulations regarding indoor air quality, in many countries of the world the monitoring of VOCs has become a serious task in order to avoid the environmental and health impact.[1,2] However, many instruments that have the ability to measure low concentrations of VOCs, such as gas chromatography, are large, bulky, and costly.[2,3] Therefore, new nanomaterials for low-cost, low-power, portable, selective, and user-friendly sensors to detect or distinguish various hazardous VOCs vapors are of great demand for chemical industry and indoor monitoring.[1,2]

Zinc oxide (ZnO) is a wide bandgap semiconductor (3.37 eV at room temperature), which is widely used in gas sensing and optoelectronic applications due to its low cost processing, wide variety of morphologies, as well as high exciton binding energy (60 meV).[4] Among all morphologies, the one-dimensional (1D) micro- and nanostructures of ZnO have attracted a great interest due to their high surface-to-volume ratio which leads to novel electrical, mechanical, chemical and optical properties.[5] In this context, individual 1D nanostructures are ideal nanosystems for studying the fundamental phenomena in low-dimensional systems and to fabricate nanodevices with high performances.[5,6]

For example, different investigations on electron transport in individual ZnO NWs showed that resistivity of NW is highly dependent on the surface reactions and surface states.[6–9] This gives the possibility to fabricate high performance photodetectors and gas sensors based on individual ZnO NWs.[8,10,11] For example, Lupan et al. fabricated a selective hydrogen gas (H$_2$) nanosensor with fast response at room temperature using an individual ZnO NW.[12] ZnO also has been used in a large extent in photodetectors.[13] Zhang et al. described a photodetector made of an array of electrodeposited ZnO NWs

Dr. T. Pauporté, Prof. O. Lupan
PSL Research University
Chimie ParisTech-CNRS
Institut de Recherche de Chimie Paris
UMR8247, 11 rue P. et M. Curie
75005 Paris, France
E-mail: thierry.pauporte@chimie-paristech.fr; oleg.lupan@mib.utm.md

Prof. O. Lupan, M. Hoppe, Prof. R. Adelung
Functional Nanomaterials
Institute for Materials Science
Kiel University, Kaiser Str. 2
D-24143 Kiel, Germany

iD The ORCID identification number(s) for the author(s) of this article can be found under https://doi.org/10.1002/pssa.201700824.

DOI: 10.1002/pssa.201700824

Prof. O. Lupan, V. Postica
Department of Microelectronics and Biomedical Engineering
Technical University of Moldova
168 Stefan cel Mare Av.
MD-2004 Chisinau, Republic of Moldova

Prof. L. Chow
Department of Physics
University of Central Florida
Orlando, FL 32816-2385, USA

ADVANCED
SCIENCE NEWS
www.advancedsciencenews.com

physica
pssa
status solidi

www.pss-a.com

with a responsivity above $10^4 A W^{-1}$,[14] whereas Soci et al. fabricated a UV photodetector with high internal gain ($G \approx 10^8$) using an individual ZnO NW.[11]

Further improvements in sensing performances of individual ZnO NWs have been achieved by different methods such as: (i) use of thinner NWs; (ii) doping with different metals; (iii) surface functionalization with noble metals, other metal oxides and different polymers; (iv) using piezoelectric properties of ZnO and (vi) the formation of Schottky contacts.[10,12,15–18] It was demonstrated that the diameter of the NW has an influence on the photocarrier relaxation behavior due to higher dominance of surface band bending.[19] Yang et al. demonstrated that the sensitivity of an individual ZnO micro-/nanowire photodetector can be enhanced by the piezo-phototronic effect.[17] Zhou et al. observed that the formation of a single Schottky contact to an individual ZnO NW can greatly enhance the UV sensitivity (by about four orders of magnitude), as well as the reset time (from $\approx 417 s$ to $\approx 0.8 s$).[18] In this case the electrical properties of the device is dominantly controlled by the characteristics of the Schottky contact which forms the local electric-field highly sensitive to light irradiation, adsorbed charged biomolecules, adsorbed gases, etc. at or near the Schottky barrier area.[20]

Among these methods, the doping of ZnO one seems to be the most attractive due to its simplicity. It can be performed during the nanostructures growth process with the absence of additional technological steps.[10] Among all potential doped materials, Al-doped ZnO (AZO) has been widely studied, mainly as thin films, for high performance optoelectronic applications.[21–25] Al doping is known to enhance the carrier density with a donor-acceptor system formed by the trivalent Al^{3+} occupation of Zn sites, thus greatly enhancing the conductivity.[22] However, this approach has been mainly developed for AZO thin films.

The aim of the present paper is to investigate the UV and gas sensing properties of individual ZnO:Al NWs. We have used individual undoped and Al-doped NWs with practically the same aspect ratio in order to exclude such factors as (i) the influence of potential barriers as in the case of NWs arrays and (ii) influence of aspect ratio induced by doping or other factors, which can greatly change the sensing properties. Therefore, we can study mainly the influence of the Al-doping on the sensing properties of ZnO NWs.

In this work, the Al-doped ZnO NWs arrays were grown on glass sheets coated with FTO by the electrochemical deposition method for the application in nanosensors. The micro-Raman and transmission spectra were investigated. The prepared NWs have been detached and individual NWs have been integrated into sensing devices using FIB/SEM equipment. Their room temperature UV and gas sensing properties have been evaluated.

2. Experimental Section

2.1. Synthesis of Al-Doped ZnO NW Arrays

Al-doped ZnO NW arrays were grown on glass sheets coated with F-doped polycrystalline SnO_2 (FTO), with a resistance of $10 \Omega/\square$, by the electrochemical deposition method.[10,16,26–29] FTO substrates were purchased from Asahi glass. The deposition was performed at 90 °C in a classical three-electrode electrochemical cell using a solution containing 0.2 mM $ZnCl_2$, 0.1 M KCl as supporting electrolyte and a continuous bubbling of oxygen in the solution bath.[10,16,26–29] The electrodeposition was performed at a constant applied potential of − 1.0 V versus the saturated calomel electrode (SCE) using an Autolab PGSTAT30 potentiostat/galvanostat monitored by the GPES AutoLab software.[10,16,26–29] The glass/FTO substrate was used as the working electrode and was rotated at a constant speed of 300 rotations/min during electrodeposition. The deposition time was about 7000 s for all the samples.

Two concentrations of $Al_2(SO_4)_3$ (≥98% $Al_2(SO_4)_3 \cdot H_2O$, Aldrich), namely 20 and 40 μM, were investigated in this work. All the samples were post-deposition annealed at 300 °C in air for 20 min.[27] More details on the electrochemical synthesis of doped ZnO NWs are presented in previous works.[26,28–30]

2.2. Characterization and Device Fabrication

The morphological, micro-Raman and optical characterizations were performed as was described previously.[30] For the device fabrication, the nanowires were detached from the glass/FTO substrate using an ultrasonic equipment and spread on a SiO_2 (300 nm in thickness) coated Si wafers pre-patterned with Cr/Au contact pads. Individual NWs were contacted on their both ends by platinum contacts using a focused ion beam/scanning electron microscopy (FIB/SEM) equipment according to the procedure described by Lupan et al.[31–33] More details on chip design and configuration of Au/Cr electrodes are presented in previous work.[32] The UV and gas sensing properties were performed in a test chamber as described in previous papers.[10,34–36] The sensor response and recovery times are defined as the necessary times to reach and recover 90% of the total responses, respectively.

3. Results and Discussion

Figure 1a shows the room temperature micro-Raman spectra of undoped and Al-doped ZnO NW arrays in the 200–800 cm^{-1} range. The Raman spectrum from the FTO substrate is also presented as a reference. The peaks originating from the FTO substrate in the Raman spectra were noted with asterisks (*) (see Figure 1a). The other peaks at ≈331, ≈385, ≈418, and ≈437 cm^{-1} can be assigned to the $E_2(high)$-$E_2(low)$, $A_1(TO)$, $E_1(TO)$, and $E_2(high)$ modes of ZnO with the wurtzite structure, respectively.[4,37] Figure 1a shows a higher intensity and a shaper band of the $E_2(high)$ mode for the sample with an aluminum salt concentration in the electrolyte of 20 μM. This shows that the crystallinity of ZnO NWs was improved by Al-doping.[23] However, a 40 μM $Al_2(SO_4)_3$ bath concentration resulted in a decrease of the peak intensity corresponding to the $E_2(high)$ mode, that is the crystallinity of ZnO:Al NWs was slightly reduced.[38] This may be due to the formation of stresses by the difference in ion size between zinc and aluminum, as well as possibly due to the segregation of the dopant.[38] Kuo et al. have reported the increase in crystallinity of ZnO:Al films with increasing doping concentrations up to 1.6 mol.%, and a

ADVANCED
SCIENCE NEWS
www.advancedsciencenews.com

physica
pss status
solidi a

www.pss-a.com
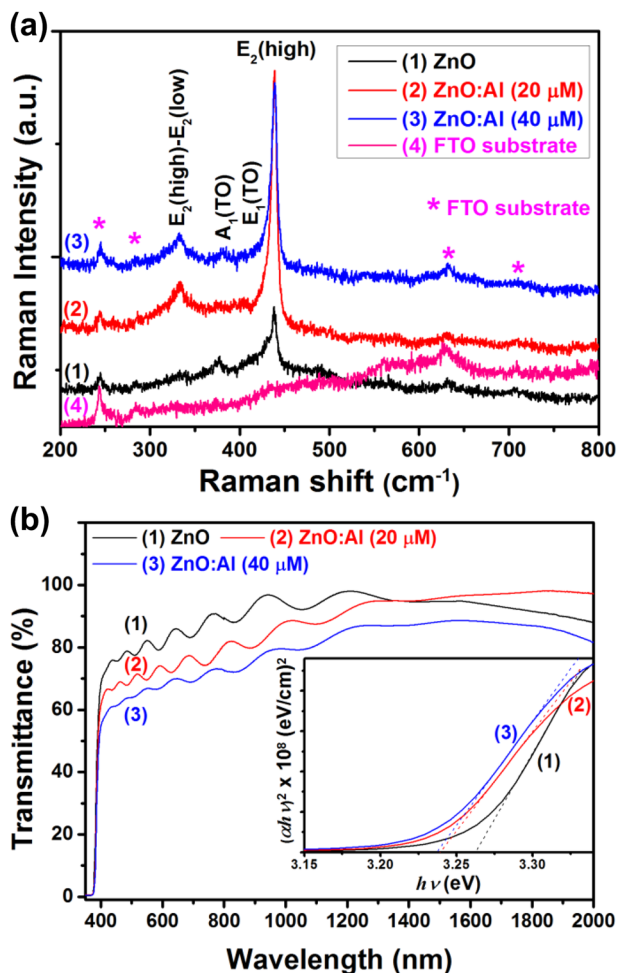
Figure 1. a) Raman spectra; and (b) transmission spectra for pure ZnO and ZnO:Al NWs arrays grown on FTO coated glass substrate. In inset is presented the $(\alpha h\nu)^2$ versus photon energy ($h\nu$) plot.

decrease in crystallinity for higher doping concentrations,[38] while Zhou et al. described a decrease in film crystallinity for content higher than 1 at.% Al.[39]

Figure 1b shows the transmission spectra of undoped and Al-doped ZnO NWs arrays. In the case of undoped ZnO NWs, the transmittance is higher than 75% in the visible region and higher than 90% in the near-infrared range. The observed interference fringes are due to the superimposition of waves that originate from the same point of the same source (a resonator being formed in the NWs).[26] By doping with Al, the transmittance is decreased to values of above 60% in visible region and about 75% in the near-infrared range (see Figure 1b). The Al-doping of ZnO has been reported to enhance the transmittance in the visible region.[40] In the present case the decrease in transmittance is probably due to the segregation of the dopant in the amorphous form.[41]

The inset from Figure 1b shows the $(\alpha h\nu)^2$ versus photon energy ($h\nu$) dependencies of undoped and Al-doped ZnO NW arrays, in order to determine the values of the optical band gap (E_g) by extrapolating the linear part of curves $(\alpha h\nu)^2$ to intercept the ($h\nu$) axis.[27] The E_g for undoped ZnO NWs is $\approx$3.26 eV. Slight

changes in the value of E_g ($\approx$3.23 eV) were observed for samples with Al-doping (see inset from Figure 1b).

Figure 2a–c show SEM images of the devices based on individual (a) ZnO, (b) ZnO:Al NW (20 µM in the electrolyte) and (c) ZnO:Al NW (40 µM), respectively. Importantly, for the sake of comparison, all devices were prepared with NWs having the same $\approx$250 nm diameter. They were contacted in FIB/SEM apparatus to pre-patterned Au/Cr contacts using Pt complex which was decomposed by the electron beam.[10,32,33] The nanosensors current–voltage characteristics are presented in Figure 2d. They show the formation of asymmetric double Schottky contacts due to the higher work functions of the Pt contacts ($\varphi = 6.1$ eV) and Au pads ($\varphi = 5.1$–5.4 eV) compared to the electron affinity of ZnO ($E_a = 4.1$ eV).[42] In the case of the ZnO:Al NWs the current is higher (see Figure 2d). This can be explained based on the increased carrier concentration.[24] The ionic radius of Al^{3+} (53 pm) smaller than that of Zn^{2+} (74 pm) and acts as a cationic dopant in the ZnO lattice.[38] The trivalent Al^{3+} ion will occupy the divalent Zn^{2+} site ($Al_{Zn}^{\bullet}$) allowing electrons to move to the conduction band easily:[23]

$$Al^{3+} + V_{Zn}^{''} \rightarrow Al_{Zn}^{\bullet} + e^- \tag{1}$$

where O_O is the oxygen from the lattice and $V_{Zn}^{''}$ is the vacancy at the Zn^{2+} site. Therefore Al^{3+} substitution in the ZnO matrix acts as an impurity and forms a point defect.[23] The increase in carrier concentration will lead to an enhancement in the electrical conductivity.[23]

Figure 2e shows the room temperature dynamic UV response to periodic illumination with UV light ($\lambda = 365$ nm). The ambient relative humidity during the measurements was measured at $\approx$30% and the power density of the UV light source was 15–20 mW cm^{-2}. The calculated UV-response for the undoped ZnO NW, ZnO:Al NW (20 µM), and ZnO:Al NW (40 µM) was $\approx$2.4, $\approx$4.8, and $\approx$4.1, respectively. So, the UV response was improved by a factor of two by Al-doping (with 20 µM), while a further increase of the aluminum salt concentration in the electrolyte solution up to 40 µM lead only to a slightly decreased UV response of an individual ZnO:Al NW. Besides the increase in the UV response, a more obvious improvement in response and recovery times can be observed (see Figure 2d). In the case of the undoped ZnO NW, the signal did not recover to initial electrical baseline even after 60 s, thus only the response time was determined to $\approx$8 s. In the case of ZnO:Al NW (20 µM) the response time did not differ significantly ($\approx$5 s), while the recovery time was $\approx$55 s. The Al-doping (with 20 µM) decreased the recovery time from a value of >60 s to $\approx$55 s. This leads to a more reproducible response, which is very important for practical applications. In the case of undoped ZnO NW the incomplete recovery of the signal after switching off the UV light led to an unstable response, that is every on/off UV irradiation cycle slightly increases the photocurrent (see Figure 2e).

It is well-known that the photoresponse of ZnO is dependent on surface adsorption and photodesorption processes of oxygen species, which are relatively slow processes.[21,35] Dhara and Giri also observed that Al-doping of ZnO NWs networks accelerates the photocurrent saturation rate, which indicates that the oxygen
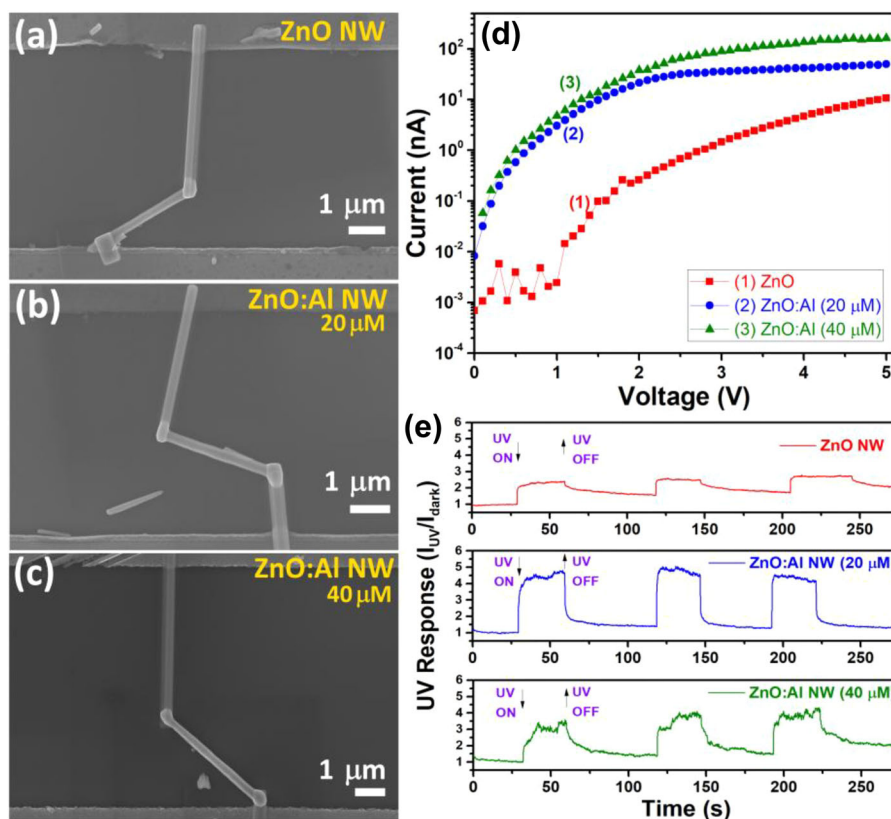
Figure 2. SEM images of the devices based on individual (a) ZnO; ZnO:Al NW (20 μM in electrolyte) and (c) ZnO:Al NW (40 μM). (d) Current − voltage characteristics (in the dark) of individual ZnO, ZnO:Al NW (20 μM) and ZnO:Al NW (40 μM). (e) Room temperature UV dynamic response of individual ZnO, ZnO:Al NW (20 μM) and ZnO:Al NW (40 μM) at 5 V applied bias voltage.

re-adsorption rate reached equilibrium instantly due to increased surface defects.[40,41] Because no investigations on defects in Al-doped ZnO NWs are provided, we tentatively propose that in our case the possible reason for faster response and recovery times can be the higher crystallinity of ZnO:Al (20 μM) compared to ZnO (see Figure 1a).[40,41] In this way, the further decrease in the crystallinity for ZnO:Al (40 μM) (see Figure 1a) can explain the slight decrease in UV response of individual ZnO:Al NW. Kim et al. also decreased the recovery time of ZnO:Al NWs network by improving the crystallinity (using thermal annealing).[40] Zhang et al. improved the photoresponse properties of ZnO thin films by Al-doping (0.5 at.%) and ascribed it to the improved crystallinity.[41] However, more details need to be investigated which will be provided in a forthcoming paper. We found that the optimal concentration of aluminum salt in the electrolyte solution in order to obtain the highest UV sensing properties of individual ZnO:Al NW was determined experimentally to be 20 μM.

The gas sensing properties of individual undoped ZnO NWs were already reported in previous works.[12,31] In this work, we will investigate only room temperature gas sensing properties of the ZnO:Al NW nanodevices shown in Figure 2b and c. All measurements were performed at 5 V applied bias. **Figure 3** shows the room temperature dynamic gas response of ZnO:Al NW (20 μM) to 1000 ppm of ethanol, 2-propanol, *n*-butanol, and ammonia vapors. It can be observed that in all cases, a drift of the

electrical baseline (decrease in current before introduction of vapors in test chamber) was observed. This can be explained based on oxygen adsorption due to self-heating effect as a result of relatively high applied bias.[43] The gas response (R) was calculated as $R = \left[\left(I_g - I_a \right) / I_a \right] \cdot 100\%$, where I_g and I_a is the current under exposure to gas and air, respectively. The calculated gas response to 1000 ppm of ethanol, 2-propanol, *n*-butanol, and ammonia vapors for ZnO:Al NW (20 μM) was ≈70, ≈48, ≈30, and ≈22%, respectively. Thus, the sensor response decreases significantly with the alkyl chain length of the alcohols compounds. The response time was ≈10 s in all cases with a reversible response (recovery time of 30–40 s), except for ammonia sensing (see Figure 3d). This can be explained based on the induced self-heating effect due to the relatively high applied bias of 5 V.[43,44] The same effect has been also observed by other research groups.[43,44] It was demonstrated that the self-heating effect is more dominant in the case of thinner individual nanostructures.[43,44] The presence of a substrate under the nanostructure is also important because it leads to heat dissipation and decreases the local operating temperature.[45–47]

Figure 4a shows the room temperature gas response of a ZnO:Al NW (20 μM) and a ZnO:Al NW (40 μM) to different concentrations of ethanol vapors (down to 50 ppm) in order to find out what concentration leads to a higher gas response. It can be observed that as in the case of UV response, the ZnO:Al NW (20 μM) possess a higher gas response to ethanol vapors
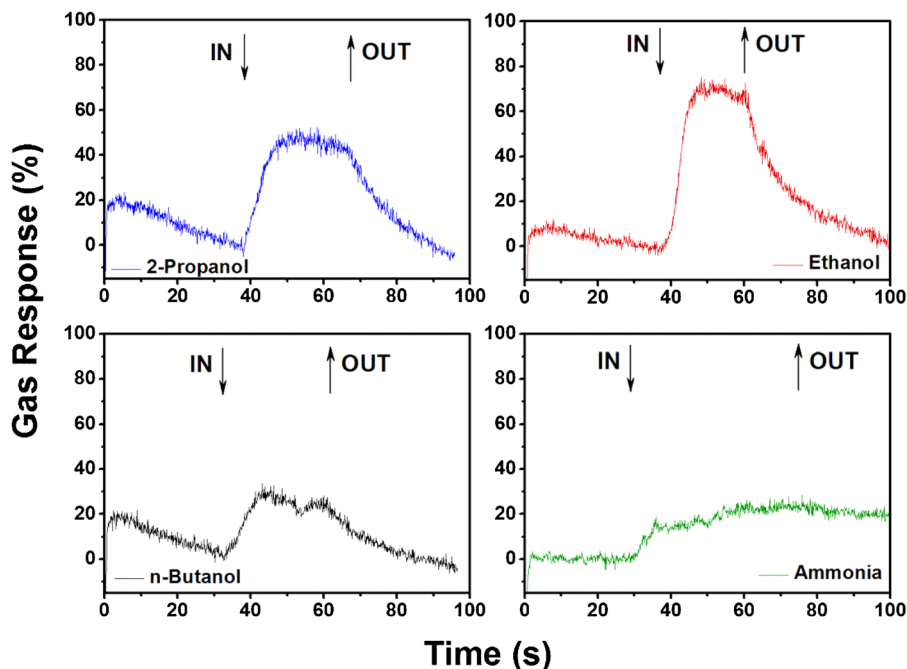
Figure 3. Dynamic gas response of ZnO:Al NW at room temperature and 5 V applied bias voltage to 1000 ppm of: (a) 2-propanol, (b) ethanol, (c) *n*-butanol, and (d) ammonia.
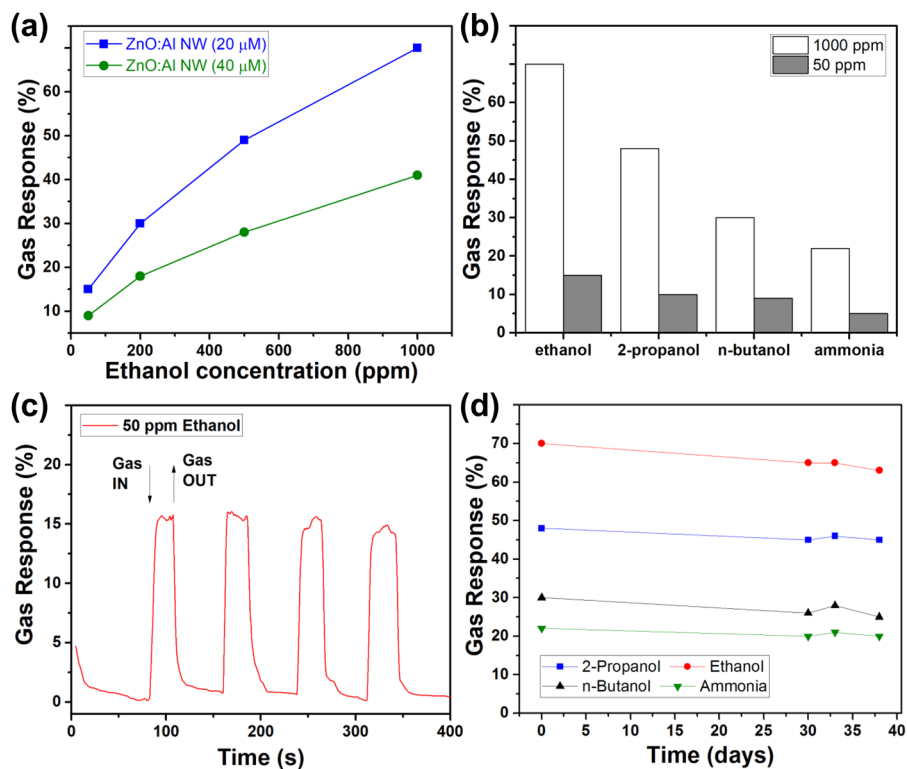
Figure 4. a) Gas response of ZnO:Al NW (20 and 40 µM in solution) to different concentrations of ethanol vapors. b) Gas response of ZnO:Al NW (20 µM) to 1000 and 50 ppm of ethanol, 2-propanol, *n*-butanol and ammonia vapors. c) The dynamic response of ZnO:Al NW (20 µM in electrolyte) to 50 ppm of ethanol vapors. d) Gas response versus time of ZnO:Al NW at room temperature and 5 V applied bias voltage to 1000 ppm of 2-propanol, ethanol, *n*-butanol, and ammonia.

Table 1. VOCs sensing properties of other nanostructures of semiconducting oxides and polymers.

Sensing individual structure	Diameter [nm]	Concentration (ppm)				Gas response (I_g/I_{air} or R_{air}/R_{gas})	Operating temp. [°C]	Response time [s]	Recovery time [s]
		EtOH	2-Propanol	n-Butanol	NH$_3$				
Single MoO$_3$ NB[32]	≈100	100	–	–	–	≈1.23	100	15	25–30
Single ZnO NW[12]	≈100	–	–	–	100	≈1.1	RT	–	–
Single ZnO ND (UV activated)[50]	–	200	–	–	–	≈30	350	10	15
Hierarchical ZnO NDs[51]	–	100	–	–	–	≈17	425	2	4
		–	–	–	100	≈10	425	–	–
Single Pt/CeO$_2$ NW[52]	≈50	200	–	–	–	≈1.25	RT	–	–
Single CuO NW[53]	≈100	500	–	–	–	≈1.6$^{a)}$	200	–	–
Individual SWCNT[54]	≈1.4	–	–	–	10 000	≈100$^{a)}$	RT	≈60–120	–
Single polypyrrole NW[55]	≈300	–	–	–	300	≈1.2$^{a)}$	RT	≈600	–
Single polyaniline NW[56]	≈300	–	–	–	100	≈55$^{a)}$	RT	≈900	–
ZnO:Al NW (this work)	≈250	1000	–	–	–	≈1.7	RT	≈10	30–40
		50	–	–	–	≈1.15	RT	–	–
		–	1000	–	–	≈1.5	RT	≈10	30–40
		–	–	1000	–	≈1.3	RT	≈10	30–40
		–	–	–	1000	≈1.22	RT	≈10	30–40

$^{a)}$Gas response was defined as R_{gas}/R_{air} or I_{air}/I_{gas} due to p-type response.

compared to ZnO:Al NW (40 μM). The gas responses to 50, 200, 500, and 1000 ppm ethanol vapors for ZnO:Al NW (20 μM) are ≈15, ≈30, ≈49, and ≈70%, respectively, and for ZnO:Al NW (40 μM) ≈9, ≈18, ≈28, and ≈41%, respectively.

Figure 4b shows the gas response to 1000 and 50 ppm of ethanol, 2-propanol, n-butanol, and ammonia vapors for ZnO:Al NW (20 μM), showing that a ZnO:Al NW can detect VOCs vapors even at much lower concentrations of VOCs (50 ppm). The gas response to 50 ppm of ethanol, 2-propanol, n-butanol and ammonia vapors is ≈15, ≈10, ≈9, and ≈5%, respectively. The repeatability of sensors is also the important parameter, especially for practical applications. Figure 4c shows the gas response of ZnO:Al NW (20 μM) to several pulses of 50 ppm ethanol, demonstrating good repeatability.

This shows that individual ZnO:Al NWs can be used as room temperature gas sensors for detection of volatile organic compounds (VOCs) vapors, which are employed in a large extent in industry (paints, coatings...) and are the main contributors to indoor air pollution.[48] Due to their high vapor pressure at room temperature and high flammability, it is very important to detect VOCs vapors with sensors which are able to work at room temperature.[49] Figure 4d shows the long-term stability of ZnO:Al NW, demonstrating that response to measured VOCs is stable during time, i.e. without essential change in response. This can be explained based on room temperature operation of devices. Previous studies demonstrated that operation at high operating temperatures results in poor long-term stability due to the deterioration of sensing properties.[12,34] Therefore, the device fabricated using individual ZnO:Al NW can be used for further development of indoor air quality monitors.

Table 1 shows the VOCs sensing properties of other nanostructures of semiconductor oxides and polymers. It can be observed that most of results with higher response are operated at temperatures higher than room temperature (RT). This is a major disadvantage because in this case the integration of micro-heaters in the device in needed. In the case of polymers or single walled carbon nanotube, higher room temperature responses are reported, however, these systems require very long recovery times up to 10 min. Therefore, in our case, the RT operation of ZnO:Al NWs with a relatively fast response is very attractive for practical applications.

The gas sensing mechanism can be explained using the ionosorption model[57] as follows. Under exposure to ambient air at room temperature, oxygen molecules adsorb on the surface of NW by capturing electrons and forming an electron-depleted layer with higher resistivity at the surface of the NW ($O_2(g) + e^- \rightarrow O_2^-(ads)$ and $O_2^-(ads) + e^- \rightarrow 2O^-(ads)$).[10,57] This leads to the narrowing of the NW conduction channel, that is a decrease in the current of the device. Once the VOCs vapors are introduced in the test chamber, the oxidation reaction takes place on the surface of the NW as follows:[58]

$$VOC + O^-(ads) \rightarrow VOC - O + e^-.$$
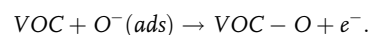
The release of electrons leads to the narrowing of the electron-depleted layer at the surface of the NW, that is a widening of the conduction channel.[10] This leads to an increase in the current flowing through the NW. More details on gas sensing mechanism of individual NW are presented in our previous works.[10,12] The increase in VOCs sensing

properties, especially to ethanol vapors of ZnO micro- and nanostructures by doping with Al has been reported by several authors.[59–61] The improvements in VOCs sensing properties of Al-doped ZnO NW compared to individual undoped ZnO NW can be explained as follow. Al-doping leads to the generation of more oxygen vacancies-related defects after substitution of Al^{3+} for Zn^{2+} ions in the ZnO lattice (see Eq. (1)).[61,62] We can extrapolate that more oxygen species adsorb on the surface of ZnO:Al NW which leads to higher reactivity of the NW surface, that is higher gas response. Bai et al. also observed that Al-doping in flower-like ZnO nanostructures leads to enhancement of sensing properties and explained this based on intrinsic defect changes and electronic interaction between the element and dopant confirmed by room temperature photoluminescence and X-ray photoelectron spectroscopy analysis.[62] Li et al. also investigated the effect of oxygen vacancy-related defect on the gas sensitivity for Al-doped ZnO tetrapods and observed that the rich oxygen vacancies provide the preferential adsorption sites for the ethoxy groups dissociated by ethanol leading to larger modulation of electron depletion region, that is gas response.[63] This mechanism could also explain our observation of an increased response to VOCs of Al-doped ZnO NW.

4. Conclusions

In summary, Al-doped ZnO NWs were grown on a FTO coated glass substrate by ECD. The micro-Raman and transmission spectra demonstrated good crystallinity of the NWs. Individual NWs with a diameter of $\approx 250\,nm$ were integrated into photodetector and sensor devices using a FIB/SEM equipment by contacting an individual NW to pre-patterned pad electrodes (Au/Cr) by Pt. UV sensing measurements demonstrated improved performances of Al-doped ZnO NWs compared to undoped ones. The UV response of doped NW $(20\,\mu M)$ was increased by about two times of magnitude (to ≈ 4.8), while the recovery time was markedly reduced from a value of $>60\,s$ to $\approx 55\,s$. The improved UV sensing properties were attributed to increased crystallinity, which was demonstrated by Raman spectra. In the case of gas sensing, we have shown that individual ZnO:Al NW $(20\,\mu M)$ can detect VOCs vapors, such as 2-propanol, n-butanol, and ethanol at room temperature within $\approx 10\,s$ with good recovery of signal (in 30 to 40 s). Our results are promising and important for room temperature indoor air quality monitoring applications.

Conflict of Interest

The authors declare no conflict of interest.

[1] M. Matsuguchi, T. Uno, *Sens. Actuators B* **2006**, *113*, 94.

[2] C. Chen, K. Driggs Campbell, I. Negi, R. A. Iglesias, P. Owens, N. Tao, F. Tsow, E. S. Forzani, *Atmos. Environ.* **2012**, *54*, 679.

[3] B. Pejcic, P. Eadington, A. Ross, *Environ. Sci. Technol.* **2007**, *41*, 6333.

[4] A. B. Djurišić, A. M. C. Ng, X. Y. Chen, *Prog. Quantum Electron.* **2010**, *34*, 191.

[5] W. Zhong Lin, *J. Phys.: Condens. Matter* **2004**, *16*, R829.

[6] Q. H. Li, Q. Wan, Y. X. Liang, T. H. Wang, *Appl. Phys. Lett.* **2004**, *84*, 4556.

[7] Z. Fan, D. Wang, P.-C. Chang, W.-Y. Tseng, J. G. Lu, *Appl. Phys. Lett.* **2004**, *85*, 5923.

[8] Q. H. Li, Y. X. Liang, Q. Wan, T. H. Wang, *Appl. Phys. Lett.* **2004**, *85*, 6389.

[9] Z.-M. Liao, K.-J. Liu, J.-M. Zhang, J. Xu, D.-P. Yu, *Phys. Lett. A* **2007**, *367*, 207.

[10] O. Lupan, V. Cretu, V. Postica, M. Ahmadi, B. R. Cuenya, L. Chow, I. Tiginyanu, B. Viana, T. Pauporté, R. Adelung, *Sens. Actuators B* **2016**, *223*, 893.

[11] C. Soci, A. Zhang, B. Xiang, S. A. Dayeh, D. P. R. Aplin, J. Park, X. Y. Bao, Y. H. Lo, D. Wang, *Nano Lett.* **2007**, *7*, 1003.

[12] O. Lupan, V. V. Ursaki, G. Chai, L. Chow, G. A. Emelchenko, I. M. Tiginyanu, A. N. Gruzintsev, A. N. Redkin, *Sens. Actuators B* **2010**, *144*, 56.

[13] O. Lupan, S. Koussi-Daoud, B. Viana, T. Pauporte, *RSC Adv.* **2016**, *6*, 68254.

[14] H. Zhang, A. V. Babichev, G. Jacopin, P. Lavenus, F. H. Julien, A. Yu. Egorov, J. Zhang, T. Pauporté, M. Tchernycheva, *J. Appl. Phys* **2013**, *114*, 234505.

[15] C. S. Lao, M.-C. Park, Q. Kuang, Y. Deng, A. K. Sood, D. L. Polla, Z. L. Wang, *J. Am. Chem. Soc.* **2007**, *129*, 12096.

[16] L. Peng, L. Hu, X. Fang, *Adv. Mater.* **2013**, *25*, 5321.

[17] Q. Yang, X. Guo, W. Wang, Y. Zhang, S. Xu, D. H. Lien, Z. L. Wang, *ACS Nano* **2010**, *4*, 6285.

[18] J. Zhou, Y. Gu, Y. Hu, W. Mai, P.-H. Yeh, G. Bao, A. K. Sood, D. L. Polla, Z. L. Wang, *Appl. Phys. Lett.* **2009**, *94*, 191103.

[19] M.-W. Chen, J. R. D. Retamal, C.-Y. Chen, J.-H. He, *IEEE Electron Device Lett.* **2012**, *33*, 411.

[20] Y. Hu, J. Zhou, P.-H. Yeh, Z. Li, T.-Y. Wei, Z. L. Wang, *Adv. Mater.* **2010**, *22*, 3327.

[21] S. Dhara, P. K. Giri, *Chem. Phys. Lett.* **2012**, *541*, 39.

[22] Y. Feng, W. Hou, X. Zhang, P. Lv, Y. Li, W. Feng, *J. Phys. Chem. C* **2011**, *115*, 3956.

[23] D. D. Lin, H. Wu, W. Pan, *Adv. Mater.* **2007**, *19*, 3968.

[24] X. Liu, K. Pan, W. Li, D. Hu, S. Liu, Y. Wang, *Ceram. Int.* **2014**, *40*, 9931.

[25] R.-C. Wang, H.-Y. Lin, C.-H. Wang, C.-P. Liu, *Adv. Funct. Mater.* **2012**, *22*, 3875.

[26] O. Lupan, T. Pauporté, L. Chow, G. Chai, B. Viana, V. V. Ursaki, E. Monaico, I. M. Tiginyanu, *Appl. Surf. Sci.* **2012**, *259*, 399.

[27] O. Lupan, T. Pauporté, L. Chow, B. Viana, F. Pellé, L. K. Ono, B. Roldan Cuenya, H. Heinrich, *Appl. Surf. Sci* **2010**, *256*, 1895.

[28] O. Lupan, T. Pauporté, T. Le Bahers, I. Ciofini, B. Viana, *J. Phys. Chem. C* **2011**, *115*, 14548.

ADVANCED SCIENCE NEWS

www.advancedsciencenews.com

physica
pss status solidi a
www.pss-a.com

[29] O. Lupan, T. Pauporté, B. Viana, P. Aschehoug, *Electrochim. Acta* **2011**, *56*, 10543.

[30] T. Pauporté, O. Lupan, J. Zhang, T. Tugsuz, I. Ciofini, F. Labat, B. Viana, *ACS Appl. Mater. Interfaces* **2015**, *7*, 11871.

[31] O. Lupan, G. Chai, L. Chow, *Microelectron. Eng.* **2008**, *85*, 2220.

[32] O. Lupan, V. Cretu, M. Deng, D. Gedamu, I. Paulowicz, S. Kaps, Y. K. Mishra, O. Polonskyi, C. Zamponi, L. Kienle, V. Trofim, I. Tiginyanu, R. Adelung, *J. Phys. Chem. C* **2014**, *118*, 15068.

[33] O. Lupan, V. Postica, N. Wolff, O. Polonskyi, V. Duppel, V. Kaidas, E. Lazari, N. Ababii, F. Faupel, L. Kienle, R. Adelung, *Small* **2017**, *13*, 1602868.

[34] O. Lupan, V. Postica, F. Labat, I. Ciofini, T. Pauporté, R. Adelung, *Sens. Actuators B* **2018**, *254*, 1259.

[35] V. Postica, I. Hölken, V. Schneider, V. Kaidas, O. Polonskyi, V. Cretu, I. Tiginyanu, F. Faupel, R. Adelung, O. Lupan, *Mater. Sci. Semicond. Process.* **2016**, *49*, 20.

[36] O. Lupan, V. Cretu, V. Postica, O. Polonskyi, N. Ababii, F. Schütt, V. Kaidas, F. Faupel, R. Adelung, *Sens. Actuators B* **2016**, *230*, 832.

[37] R. Cuscó, E. Alarcón-Lladó, J. Ibáñez, L. Artús, J. Jiménez, B. Wang, M. J. Callahan, *Phys. Rev. B* **2007**, *75*, 165202.

[38] S. H. Jeong, J. W. Lee, S. B. Lee, J. H. Boo, *Thin Solid Films* **2003**, *435*, 78.

[39] H. Zhou, D. Yi, Z. Yu, L. Xiao, J. Li, *Thin Solid Films* **2007**, *515*, 6909.

[40] K.-P. Kim, D. Chang, S. K. Lim, S.-K. Lee, H.-K. Lyu, D.-K. Hwang, *Curr. Appl. Phys.* **2011**, *11*, 1311.

[41] Y. Zhang, J. Xu, S. Shi, S. Gao, C. Wang, X. Zhang, S. Yin, L. Li, *ACS Appl. Mater. Interfaces* **2016**, *8*, 22647.

[42] Z. L. Wang, J. Song, *Science* **2006**, *312*, 242.

[43] A. Jae-Hyuk, Y. Jeonghoon, M. Dong-Il, C. Yang-Kyu, P. Inkyu, *Nanotechnology* **2015**, *26*, 095501.

[44] J. D. Prades, R. Jimenez-Diaz, F. Hernandez-Ramirez, S. Barth, A. Cirera, A. Romano-Rodriguez, S. Mathur, J. R. Morante, *Appl. Phys. Lett.* **2008**, *93*, 123110.

[45] R. Rhyner, M. Luisier, *Nano Lett.* **2016**, *16*, 1022.

[46] T. Kawano, H. C. Chiamori, M. Suter, Q. Zhou, B. D. Sosnowchik, L. Lin, *Nano Lett.* **2007**, *7*, 3686.

[47] J. Seo, Y. Lim, H. Shin, *Sens. Actuators B* **2017**, *247*, 564.

[48] V. K. Tomer, S. Duhan, *J. Mater. Chem. C* **2016**, *4*, 1033.

[49] S. Öztürk, A. Kösemen, Z. A. Kösemen, N. Kılınç, Z. Z. Öztürk, M. Penza, *Sens. Actuators B* **2016**, *222*, 280.

[50] M. R. Alenezi, A. S. Alshammari, K. D. G. I. Jayawardena, M. J. Beliatis, S. J. Henley, S. R. P. Silva, *J. Phys. Chem. C* **2013**, *117*, 17850.

[51] M. R. Alenezi, S. J. Henley, N. G. Emerson, S. R. P. Silva, *Nanoscale* **2014**, *6*, 235.

[52] L. Liao, H. X. Mai, Q. Yuan, H. B. Lu, J. C. Li, C. Liu, C. H. Yan, Z. X. Shen, T. Yu, *J. Phys. Chem. C* **2008**, *112*, 9061.

[53] L. Liao, Z. Zhang, B. Yan, Z. Zheng, Q. L. Bao, T. Wu, C. M. Li, Z. X. Shen, J. X. Zhang, H. Gong, J. C. Li, T. Yu, *Nanotechnol.* **2009**, *20*, 085203.

[54] J. Kong, N. R. Franklin, C. Zhou, M. G. Chapline, S. Peng, K. Cho, H. Dai, *Science* **2000**, *287*, 622.

[55] S. C. Hernandez, D. Chaudhuri, W. Chen, N. V. Myung, A. Mulchandani, *Electroanal.* **2007**, *19*, 2125.

[56] H. Liu, J. Kameoka, D. A. Czaplewski, H. G. Craighead, *Nano Lett.* **2004**, *4*, 671.

[57] N. Bârsan, U. Weimar, *J. Phys.: Condens. Matter* **2003**, *15*, R813.

[58] B. L. Zhu, C. S. Xie, W. Y. Wang, K. J. Huang, J. H. Hu, *Mater. Lett.* **2004**, *58*, 624.

[59] Z. Yang, Y. Huang, G. Chen, Z. Guo, S. Cheng, S. Huang, *Sens. Actuators B* **2009**, *140*, 549.

[60] F. Paraguay-Delgado, M. Miki-Yoshida, J. Morales, J. Solis, W. Estrada-Lopez, *Thin Solid Films* **2000**, *373*, 137.

[61] M. Zhao, X. Wang, J. Cheng, L. Zhang, J. Jia, X. Li, *Current Appl. Phys.* **2013**, *13*, 403.

[62] S. Bai, T. Guo, Y. Zhao, R. Luo, D. Li, A. Chen, C. C. Liu, *J. Mater. Chem. A* **2013**, *1*, 11335.

[63] L. M. Li, Z. F. Du, T. H. Wang, *Sens. Actuators B* **2010**, *147*, 165.